Hindawi
International Journal of Chemical Engineering
Volume 2019, Article ID 5743590, 13 pages
https://doi.org/10.1155/2019/5743590

Research Article

Column Efficiency of Fluoride Removal Using Quaternized Palm Kernel Shell (QPKS)

Ayu Haslija Abu Bakar,[1,2] **Luqman Chuah Abdullah**,[1,3] **Nur Amirah Mohd Zahri**,[4] **and Ma'an Alkhatib**[5]

[1]*Department of Chemical and Environmental Engineering, Faculty of Engineering, Universiti Putra Malaysia, 43400 UPM Serdang, Selangor D.E., Malaysia*
[2]*Department of Chemical and Petroleum Engineering, Faculty of Engineering, Technology & Built Environment, UCSI University, 56000 Cheras, Kuala Lumpur, Malaysia*
[3]*Institute of Tropical Forestry and Forest Products (INTROP), Universiti Putra Malaysia, 43400 UPM Serdang, Selangor D.E., Malaysia*
[4]*Department of Mechanical Engineering, Faculty of Engineering, Universiti Malaya, 50603 Kuala Lumpur, Malaysia*
[5]*Biotechnology Engineering Department, Kulliyyah of Engineering, International Islamic University Malaysia (IIUM), Jalan Gombak, 53100 Kuala Lumpur, Malaysia*

Correspondence should be addressed to Ayu Haslija Abu Bakar; chik_ija@yahoo.com

Received 28 November 2018; Revised 9 March 2019; Accepted 17 March 2019; Published 12 May 2019

Academic Editor: Eric Guibal

In this research, the adsorption potential of quaternized palm kernel shell (QPKS) to remove F^- from aqueous solution was investigated using fixed-bed adsorption column. Raw palm kernel shell waste was reacted with 3-chloro-2-hydroxypropyl trimethylammonium chloride (CHMAC) in order to modify the surface charge. The effects of inlet F^- concentrations (2–12 mg/l) and QPKS bed height (2–10 cm) with optimum pH (pH = 3) on the breakthrough characteristics of the adsorption system were determined. In the fixed-bed column, breakthrough time increases with increasing bed height due to increasing amount of active site on adsorbents to adsorb the fluoride ion. Decreasing trend of breakthrough values was obtained with increasing initial fluoride concentration due to greater driving force for the transfer process to overcome the mass transfer resistance in the column. The adsorptions were fitted to three well-established fixed-bed adsorption models, namely, Thomas, Yoon–Nelson, and Adams–Bohart models. The results fitted well to the Thomas and Yoon–Nelson models with correlation coefficient, $R^2 \geq 0.96$.

1. Introduction

Today, hazardous waste has become one of the environmental problems. Hazardous waste can be classified into different types of waste mainly nuclear waste, industrial waste, universal waste, medical waste, and construction waste. Hazardous waste can be in the form of solid, liquid, and gas which are not easily disposed due to its corrosiveness, toxicity, and ignitability. Fluoride is one of the hazardous wastes commonly produced by industries using hydrofluoric acid as cleaning agents or etchant. Industries manufacturing glass and ceramic, semiconductors, electroplating, coal-fired power stations, beryllium extraction plants, brick and iron works, and aluminium smelters discharge high concentration of fluoride [1]. High concentration of fluoride ions in water is mainly affected by natural minerals and industrial activities. Lv et al. [2] reported that concentration of fluoride in the wastewater from Zhejiang Juhua Fluorine Chemical Co. Ltd. exceeds 1000 mg/L (pH = 5–7). According to Ruan et al. [3], most natural rocks and minerals contain large quantities of fluoride which are released as fluoride ions into water contributing to levels of fluoride concentrations rise in water that exceed the acceptable limit set by the WHO which is 1.5 mg/L. Therefore, fluoride content in wastewater and drinking water should be reduced in order to improve the health quality.

The standards prescribed by various regulatory bodies for fluoride concentration in drinking water are different according to their climatic conditions. According to the WHO, the standard prescribed for fluoride ion concentration in drinking water is 1.5 mg/L. Fluoride in smaller doses (0.8–1.0 mg/L) helps to prevent dental caries particularly among children below eight years of age. Fluoride in higher concentration causes dental fluorosis (1.5–2.0 mg/L) and skeletal fluorosis (>3.0 mg/L) [4]. Chemically, fluorine is the most electronegative element and is always present in a combined state as fluoride due to its high chemical reactivity. Fluoride is a great calcium-seeking element and can affect the calcified structure of bones and teeth in the human body at higher concentration, resulting in dental fluorosis or skeletal fluorosis. Fluoride toxicity can also cause nonskeletal diseases such as aches and pain in the joints, nonulcer dyspepsia, polyurea (tendency to urinate more frequently) and polydipsia (excessive thrust), muscle weakness, fatigue, and anemia with very low haemoglobin levels [5].

Over the years, many techniques and processes have been developed and used in the treatment and removal of fluoride from the contaminated water effluent. These techniques include coagulation and flocculation, chemical precipitation, the use of membranes for membrane separation, aerobic and anaerobic degradation using various microorganisms, chemical oxidation, ion exchange, electrodialysis, reverse osmosis, foam flotation, electrolysis, and adsorption [6]. Some of these techniques have been proven to be effective, although they displayed some limitations such as the excess amount of chemical usage or accumulation of highly concentrated sludge, causing disposal problems, lack of effective fluoride reduction, and sensitivity towards various wastewater inputs [7].

Amongst the processes mentioned above, the use of adsorption has been the most prominent and widely used because of its cost-effectiveness, efficiency, and technology readiness due to the fact that it produces effluents containing very low levels of dissolved organic compounds [8]. In addition, many adsorption techniques have been employed for the treatment of drinking water, as reviewed in the work reported by Tikki [9].

Adsorption is the process through which a substance, originally present in one phase, is removed from that phase of accumulation at the interface between that phase and a separate (solid) phase. It can also be referred to as the separation of components in a fluid mixture by the transfer of one or more components (known as the adsorbate) to the internal surface of a porous solid (known as the adsorbent) where they are held by intermolecular forces. However, adsorption is different from absorption in the sense that, in absorption, a substance diffuses into a liquid or solid to form a solution. Thus, the connecting term "sorption" encompasses both processes, whereas desorption is the reverse process.

Generally, the solid material that adsorbs the adsorbate is referred to the adsorbent. There are various types and classifications of adsorbents; but in general, adsorbents are classified to be either organic or inorganic adsorbents. The physical properties of adsorbents include their shape, porous structure, and specific surface area. In order to determine the type of adsorbent to be selected for a particular adsorption process, the following criteria must be taken into consideration:

(a) High capacity to reduce the amount of adsorbent needed

(b) Favourable kinetic and transport properties to allow for rapid sorption

(c) Should be thermally and chemically stable in order to allow for the preservation of both quantity and properties

(d) Good hardness and material strength

(e) Resistance to fouling

(f) Regenerative capability to allow for reuse [10]

The adsorption process is based on three steps as explained in the following by Viegas et al. [11]:

(1) Mass transfer of solute from the bulk solution through the stagnant film surroundings to the particle external surface (external or film mass transport).

(2) Mass transfer of solute within the particle (internal or intraparticle diffusion). Intraparticle diffusion may be due to pore volume diffusion (diffusion in the fluid-filled pores), surface diffusion (migration along the pore surface in which an adsorbate hops from one to another available adsorption site in a series of adsorption-desorption reactions), or a combination of both.

(3) Solute attachment onto the surface of the adsorbent surface site, adsorption.

Step (3), adsorption, is usually very rapid compared to the first two steps, and the overall rate of adsorption is therefore often controlled by the first or the second steps, whichever is slower, or a combination of both.

Adsorption process is widely used due to its effectiveness giving satisfactory results and also in terms of cost, simplicity of design, and operations [12, 13]. Many research studies have focused on the low-cost adsorbent in the removal of wastewater pollutant such as heavy metal by carbonized green mussel shell [14], modified agriculture wastes [15], aerogel adsorbent from combination of waste office paper and chitosan [16], and many more. Meanwhile, low-cost adsorbent application in fluoride removal has been studied by Singh et al. [17] who used sugarcane bagasse as an adsorbent, Ayu Haslija et al. [18] used modified palm kernel shell in batch process adsorption, Mukherjee et al. [19] synthesized zeolite adsorbent from rice husk, and Hu et al. [20] used chitosan/aluminum hydroxide bead adsorbent, and many more.

Malaysia is one of the largest producers and exporters of palm oil in the world producing a large quantity of by-products which is the palm kernel shell. According to the data obtained from the Malaysian Palm Oil Board (MPOB) which is represented in Table 1, 4.5 million tonnes of palm kernel shell (PKS) has been produced as of November 2017. This big amount could lead to a serious environmental problem if no proper waste management system is carried out.

Table 1: Production of palm kernel shell in metric tonnes (MT) until November 2017 [21].

Region	Total production (MT) from January to November	
	2016	2017
Peninsular Malaysia	2,175,971	2,636,756
Sabah/Sarawak	1,667,945	1,849,141
Malaysia	**3,843,916**	**4,485,897**

The shell is practically removed by steam treatment and mechanically crushed from the oil palm fruit. These by-products are usually burned off emitting dark smoke as well as partially carbonized fibrous particulates due to incomplete combustion leading to pollutions. Thus, to prevent the pollutions, the PKS can be further processed as the adsorbent for adsorption process.

In this research, palm kernel shell is chemically modified to act as an adsorbent for F^- removal from aqueous solution by using the fixed-bed column. Characterization analysis was done to analyze the properties of the adsorbent produced. The crucial design parameters such as inlet concentration of F^- solution and column bed height were investigated. The breakthrough curves for the adsorption of F^- were analyzed using Adams–Bohart, Thomas, and Yoon–Nelson models.

2. Materials and Methods

2.1. Materials. Palm kernel shell was obtained from Seri Ulu Langat Palm Oil Mill Sdn. Bhd., Selangor, Malaysia. 60 wt. % of sodium hydroxide (NaOH) was used for the mercerization process of palm kernel shell while 3-chloro-2-hydroxypropyl trimethylammonium chloride (CHMAC) solution used for the quaternization process. Stock solutions of F^- were prepared by dissolving appropriate amount of NaF in the deionized distilled water.

2.2. Quaternization and Experimental Setup. The quaternization process was carried out by impregnating mercerized PKS with NaOH solution and CHMAC at a ratio (w/w) of 5 H_2O : 1 sample : 1 NaOH : 4 CHMAC [22]. All chemicals were purchased from Sigma-Aldrich. The sample was then shaken at 100 rpm on a digital orbital shaker, Wise Shake SHO-2D (Wise Laboratory Instruments, Korea), for 24 hours to accelerate the reaction. After quaternization, the quaternized PKS (QPKS) was washed with 2% acetic acid solution, followed by distilled water until the solution was neutral (pH 7) to stop the reaction. The washed QPKS was dried in the oven at 60°C overnight and cooled in a desiccator for further experimental usage.

A transparent cylindrical glass column of 2 cm internal diameter and 35 cm height, as shown by Figure 1, was used to conduct the continuous column adsorption experiments. A glass wool of 0.5 mm was attached at the bottom of the column. The column performance of F^- adsorption onto QPKS was studied at different F^- concentration (2–12 mg/l) and bed height (2–10 cm) at pH 3. The pH was adjusted by adding 0.1 M HCl into the solution. Effluents were collected at the bottom of the column at regular intervals and analyzed for fluoride using UV/VIS double beam spectrophotometer (GENESYS 10 UV, USA) at a wavelength of 570 nm.

2.3. Adsorbent Analysis

2.3.1. Functional Group Analysis. Functional groups of samples and infrared (IR) spectra were determined and recorded on the Fourier-transform infrared (FTIR) spectrometer (PerkinElmer 1750X, PerkinElmer, USA). Attenuated total reflectance (ATR) technique was used for all sample measurements whereby spectra were collected based on measurements of the temporal coherence of a radiative source. The percentage of transmittance against wave number (cm^{-1}) within the range of 400–4000 cm^{-1} at room temperature was plotted for all spectra.

2.3.2. Surface Morphology and Elemental Analysis. Surface morphology and elements in of raw palm kernel shell (PKS) were analyzed and compared with quaternized PKS and PKSAC by using scanning electron microscopy with energy-dispersive X-ray (Hitachi Model S-3400N, Hitachi, Japan). SEM-EDX is a microscope that uses electrons to form images.

2.3.3. Porosity and Surface Area Analysis. Brunauer–Emmett–Teller (BET) method was used to analyze the surface area of samples. The BET surface area analyser used was AutoSorb-1 (Quantachrome Instruments, USA). Pore size distribution, average pore size, and pore volume of the samples were determined using the Barrett–Johner–Halenda (BJH) equation.

2.3.4. Crystallinity Analysis. XRD analysis was performed by PANalytical XRD instrument with Cu radiation 1.542 Å in order to identify the adsorbents' crystalline materials (e.g., minerals and inorganic compounds). The X-ray tube was operated at 45 kV and 40 mA where the 2θ angle of the diffractometer was stepped from 10° to 80° scan rate with a step size of 0.02°.

2.4. Breakthrough Profile. Breakthrough profiles were plotted for each parameter to analyze the best condition to efficiently remove fluoride by plotting C_t/C_0 against time, t (min). The maximum column capacity, q (mg/g), for a given parameter is equal to the area under the breakthrough curve.

2.5. Kinetic Models. In this research, Thomas, Yoon–Nelson, and Adams–Bohart models were used to analyze the kinetic studies. The Thomas model is based on the assumption that the process follows Langmuir kinetics of adsorption-desorption with no axial dispersion. It describes that the rate driving force obeys the second-order reversible reaction kinetics [23].

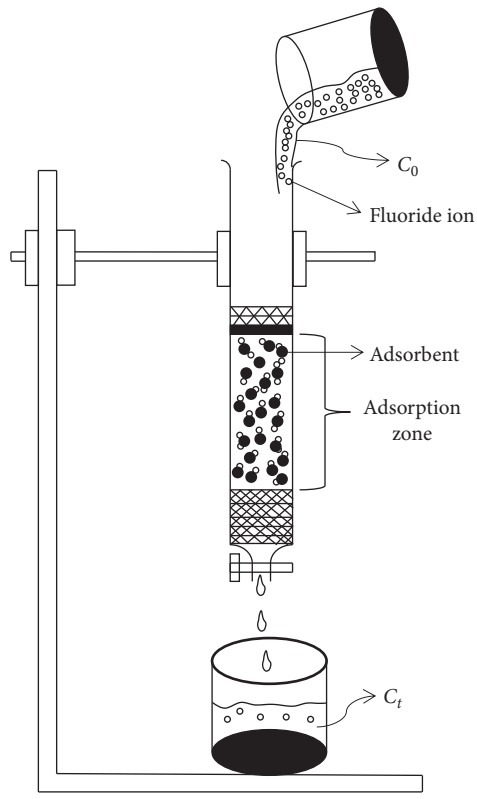

Figure 1: Schematic diagram of column.

The linearized form of the model is given as follows:

$$\ln\left(\left(\frac{C_0}{C_t}\right)-1\right)=\frac{K_{\mathrm{Th}}q_{\mathrm{e}}M}{Q}-K_{\mathrm{Th}}C_0t, \tag{1}$$

where K_{Th} is the Thomas rate constant (mL/min·mg), q_{e} is the equilibrium adsorbate uptake per g of adsorbent, C_0 is the inlet adsorbate concentration (mg/L), C_t is the outlet concentration at time t (mg/L), M is the mass of adsorbent (g), Q is the filtration velocity (mL/min), and t is the filtration time (min).

The Adams–Bohart model is used for the description of the initial part of a breakthrough curve but its validity is limited in the concentration of $C<0.5C_0$ range [24]. The mathematical equation of the model can be written as follows:

$$\ln\left(\frac{C}{C_0}\right)=\exp\left(K_{\mathrm{AB}}C_0t-K_{\mathrm{AB}}N_0\left(\frac{Z}{v}\right)\right), \tag{2}$$

where v (cm/min) is the linear flow rate, N_0 (mg/L) is the saturation concentration, K_{AB} (L/mg·min) is the kinetic constant, and Z is the bed depth of column (cm). The linear flow rate was calculated from the equation $v = Q/A$ where Q is the volumetric flow rate (ml/min) and A is the transversal area of the column (cm^2).

A prediction model bed depth service time (BDST) which focuses on the theory of surface reaction rate and prediction of column efficiency between bed height (Z) and service time (t) is based on the Adams–Bohart model. This BDST model can be used to achieve the required breakthrough at the given column condition [25]. The Adams–Bohart equation was modified by Hutchins [26] who proposed a linear relationship between bed height and service time as

$$t=\frac{N_0Z}{C_0v}-\frac{1}{K_{\mathrm{a}}C_0}\ln\left(\frac{C_0}{C_{\mathrm{b}}}-1\right), \tag{3}$$

where C_0 is the initial F^- concentration (mg/L), C_{b} is the breakthrough F ion concentration (mg/L), v is the linear velocity (cm/min), N_0 is the adsorption capacity of bed (mg/L), K_{a} is the rate constant of the BDST model (L/mg/min), t is the time (min), and Z is the bed height (cm) of the column. Equation (3) can be linearized into equation (4):

$$t=aZ-b, \tag{4}$$

where the critical bed depth, Z_0, occurs at time $t = 0$ which is the theoretical value of bed depth of the adsorbent which the effluent concentration does not exceed the breakthrough concentration (C_{b}). Therefore, when $t = 0\,(Z_0)$, equation (3) changes to equation (5):

$$Z_0=\frac{v}{K_0N_0}\ln\left(\frac{C_0}{C_{\mathrm{b}}}-1\right). \tag{5}$$

According to Mohan et al. [25], a prediction of the concentration-time profile or breakthrough curve and adsorption capacity for the effluent under given specific operating conditions is required in order to design a column for the adsorption process.

Yoon and Nelson [27] developed a model known as Yoon–Nelson model, which assumed that the rate of decrease in the probability of sorption for each adsorbate molecule was proportional to the probability of adsorbate sorption and the probability of adsorbate breakthrough on the adsorbent [28]. The model is described by the following equation:

$$\ln\left(\frac{C_t}{C_0 - C_t}\right) = k_{YN}t - k_{YN}\tau, \quad (6)$$

where k_{YN} (min^{-1}) is the Yoon–Nelson rate constant and τ (min) is the time required for 50% sorbate breakthrough.

Tofan et al. [23] stated that, according to the Yoon–Nelson model, the amount of adsorbate ion sorbed in a fixed bed is half of the total adsorbate ion entering the adsorption bed within 2τ period. Results obtained for adsorption of Cr (III) by modified hemp fibers showed that the values of the Yoon–Nelson rate constant, k_{YN}, increase as the initial concentration increases. This is probably due to the increases of competition between the sorbate species on the sorption sites by increasing initial concentration of the metal ion, which results in a higher rate of retention. It is known that k_{YN} and τ are inversely related; therefore, the time required for 50% breakthrough, τ, decreases with increasing the influent concentration of Cr(III).

3. Results and Discussion

3.1. Adsorbent Characteristic

3.1.1. Surface Morphology Analysis. Surface morphology of raw PKS and QPKS was analyzed using SEM. Figure 2(a) presents the surface of raw PKS which showed small size, uneven, and low amount of pores while the surface seems to be covered by a layer of impurities. On the other hand, Figure 2(b) shows that QPKS had more pores compared to raw PKS (Figure 2(a)) which resulted from the mercerization and quaternization process which remove impurities under alkaline condition in NaOH [29] and therefore created more pores. The quantitative data on PKS and QPKS pore size were determined using BET analysis in the subsequent part.

3.1.2. Surface Elemental Analysis. Energy-dispersive X-ray analysis is a surface elemental analysis used in conjunction with SEM. The results for PKS and QPKS are listed in Table 2.

A high percentage of nitrogen was detected in QPKS as the result of quaternization process, but was not detected in PKS. Hence, this analysis again verifies that the quaternary ammonia group (NR_4^+) reacted on the surface of QPKS, resulting in a successful synthesis.

3.1.3. Porosity and Surface Area Analysis. The adsorbent's pore characteristics are given in Table 3, which show that the average pore diameters of PKS and QPKS were 2.2 nm and 35.2 nm, respectively. Due to the size of these pores, they are classified as mesopores. Enlargement of the pore size in QPKS was due to the dissolution of impurities in NaOH solution during the pretreatment mercerization and quaternization processes.

3.1.4. Functional Group Analysis. The fundamental of FTIR analysis is to identify the functional groups exist in an organic compound. Figure 3 shows FTIR spectra of raw PKS and QPKS, where the existence of –CN, –COC (ether), and –Cl was shown in the peaks at wavenumbers of 1331 cm^{-1}, 1105 cm^{-1}, and 682 cm^{-1}, respectively, which were not present in raw PKS. In order to prove the designated peaks such as –CN, –COC, and –Cl peaks, software from Bio-Rad, KnowItAll-Academic Edition, has been applied. Figures 3(b)–3(d) show the peaks extracted from software. The existence of the –CN peak showed that the surface of PKS was successfully quaternized (NR_4^+) with CHMAC, and this is one of the main factors to enhance the adsorption of fluoride ions.

These peaks can attribute quaternization mechanism process as illustrated in Figure 4 adapted from de Lima et al. There are three reaction steps in a quaternization reaction: the interaction between cellulose and sodium hydroxide, epoxy formation from CHMAC, and the reaction between epoxide and the hydroxyl group of cellulose to produce ether with the presence of acid to stop the reaction, as shown in Figure 4.

3.1.5. Crystallinity Analysis. Pattern of XRD peaks for raw PKS and QPKS is shown in Figure 5. Figure 5(a) shows raw PKS' peak before modification in which two main peaks can be observed at $2\theta = 22^\circ$ and 35° indicating the existence of carbon and oxygen. The peak of QPKS is represented by Figure 5(b) which shows different pattern due to the quaternization process. The highest peak of QPKS is at $2\theta = 12^\circ$ which is not present in raw PKS including peak at $2\theta = 24^\circ$, 26°, and 33°. These peaks indicate the presence of nitrogen and chloride element in the QPKS base on reference database in Match software. Figure 5(c) is resulted after removing raw PKS peak from QPKS peak and clearly proves the existence of nitrogen and chloride on QPKS due to the quaternization process. This characteristic is the main factor on the adsorption of fluoride from solution.

3.1.6. Point of Zero Charge. The point of zero charge was performed to determine the surface chemistry characterisation of adsorbent. By conducting this test, the pH of the point of zero charge, pH_{pzc}, of QPKS was determined. The pH_{pzc} of the adsorbent is a very important characteristic that determines the pH when the electrical charge density on a surface is zero. From Figure 6, the pH_{pzc} of QPKS, which was the point when $\Delta pH = 0$ ($pH_{initial} = pH_{final}$) was close to pH = 4.1. At $\Delta pH < 0$, there was a net positively charge on the surface of adsorbents, which was likely to attract anions. The most negative value of ΔpH for QPKS was found at pH 3.2 (−1.01), which indicated that the

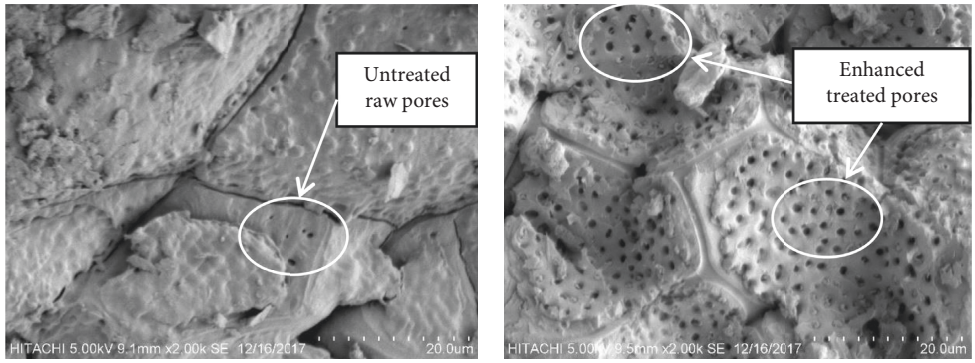

(a) (b)

Figure 2: (a) Raw palm kernel shell. (b) Quaternized palm kernel shell (QPKS).

Table 2: EDX analysis of PKS and QPKS.

Element (wt.%)	PKS (wt.%)	QPKS (wt.%)
Carbon	40.25	39.09
Oxygen	59.75	34.57
Nitrogen	0.00	24.34

Table 3: Pore characteristics of adsorbents.

Adsorbent	BET surface area (m^2/g)	Average pore diameter (nm)	Pore volume/porosity (cm^3/g)
PKS	1.93	2.200	0.003
QPKS	21.75	35.22	0.19

surface of the adsorbent was most positively charged at this pH and thus, exerted the greatest electrostatic forces of attraction for anions.

According to Railsback [31], pH below pH_{pzc} had positively charged surface due to H^+ ions being adsorbed on the surface rather than entering the low pH (H^+ rich) solution, resulting in a positively charged (H^+ rich) surface, which is a very important characteristic in adsorbing fluoride ion (F^-). In this study, the electrolyte solution used was 0.1 M $NaNO_3$, which consisted of Na^+ as cations and NO_3^- as anions, which may be adsorbed. The following equations derived from Cardenas-Peña et al. [32] showed Q^+, which represents the surface of QPKS. Hence, by combining with Railsback's [31] statement, the following equations can best describe the mechanism of the adsorption process at optimum pH:

$$\begin{aligned} QOH_{(surf)} + {NO_3}^-{}_{(aq)} &= Q^+{NO_3}^-{}_{(surf)} + OH^- \\ QOH_{(surf)} + {F}^-{}_{(aq)} &= Q^+{F}^-{}_{(surf)} + {OH}^-{}_{(aq)} \\ {Q}^+{}_{(surf)} + {F}^-{}_{(aq)} &= QF_{(surf)} \end{aligned} \quad (7)$$

Meanwhile, in the condition of high pH, which contributed of more H^+ ions in the solution, hydrofluoric acid might be produced. On the other hand, displacement of Cl^- ion from the quaternized adsorbent is replaced by F^- producing HCl in the solution. The following equation shows the possibility of the reactions to occur:

$$\begin{aligned} {H}^+{}_{(aq)} + {F}^-{}_{(aq)} &= HF_{(aq)} \\ {H}^+{}_{(aq)} + {Cl}^-{}_{(aq)} &= HCL_{(aq)} \end{aligned} \quad (8)$$

3.2. Effect of Inlet Initial F^- Concentration. Effect of initial fluoride concentration on breakthrough profile at 2, 8, and 12 mg/L with optimum pH, bed height of 6 cm, and flow rate at 4 ml/min was studied, and the results are shown in Figure 7 and Table 4. The breakthrough curve clearly showed the transfer mechanism at different initial fluoride concentrations.

Using 2 mg/l as the lowest initial concentration, breakthrough and exhausted time for each adsorbent were analyzed. The curve from Figure 7 clearly shows that QPKS achieved breakthrough time at 17.5 minute and exhausted at 23.75 minute. At initial fluoride concentration of 8 mg/L, the breakthrough time and exhausted time of QPKS were at 9.3 and 15 minutes. Meanwhile, for 12 mg/l of fluoride concentration, QPKS breakthrough at a faster rate was 5.3 minutes due to the vacant site filled up faster by fluoride ion and exhausted at 8.75 minutes.

From the analysis, it can be concluded that breakthrough time decreased with increased initial fluoride concentration. As the concentration increased, amount of adsorbate also increased; therefore, active sites were occupied at a faster rate. Adsorbate ions will saturate on adsorbent faster (exhaust) and in a shorter time to achieve the breakthrough time with increasing influent fluoride concentration due to greater mass transfer driving force for the transfer process to overcome the mass transfer resistance in the column [33–35]. Similar trend was reported by Chen et al. [33] for fluoride removal using Kanuma mud and hydrous ferric oxide by Nur et al. [34]. Table 1 summarizes all the breakthrough and exhaust time for QPKS.

3.3. Effects of Bed Height. Figure 8 shows the breakthrough profile of bed heights at different bed heights. The breakthrough curve for 2 cm bed height had steeper curve as compared to curve at 6 and 10 cm bed height. The curve trend of bed height effect was observed to decrease with higher bed height but the higher the bed height, the longer

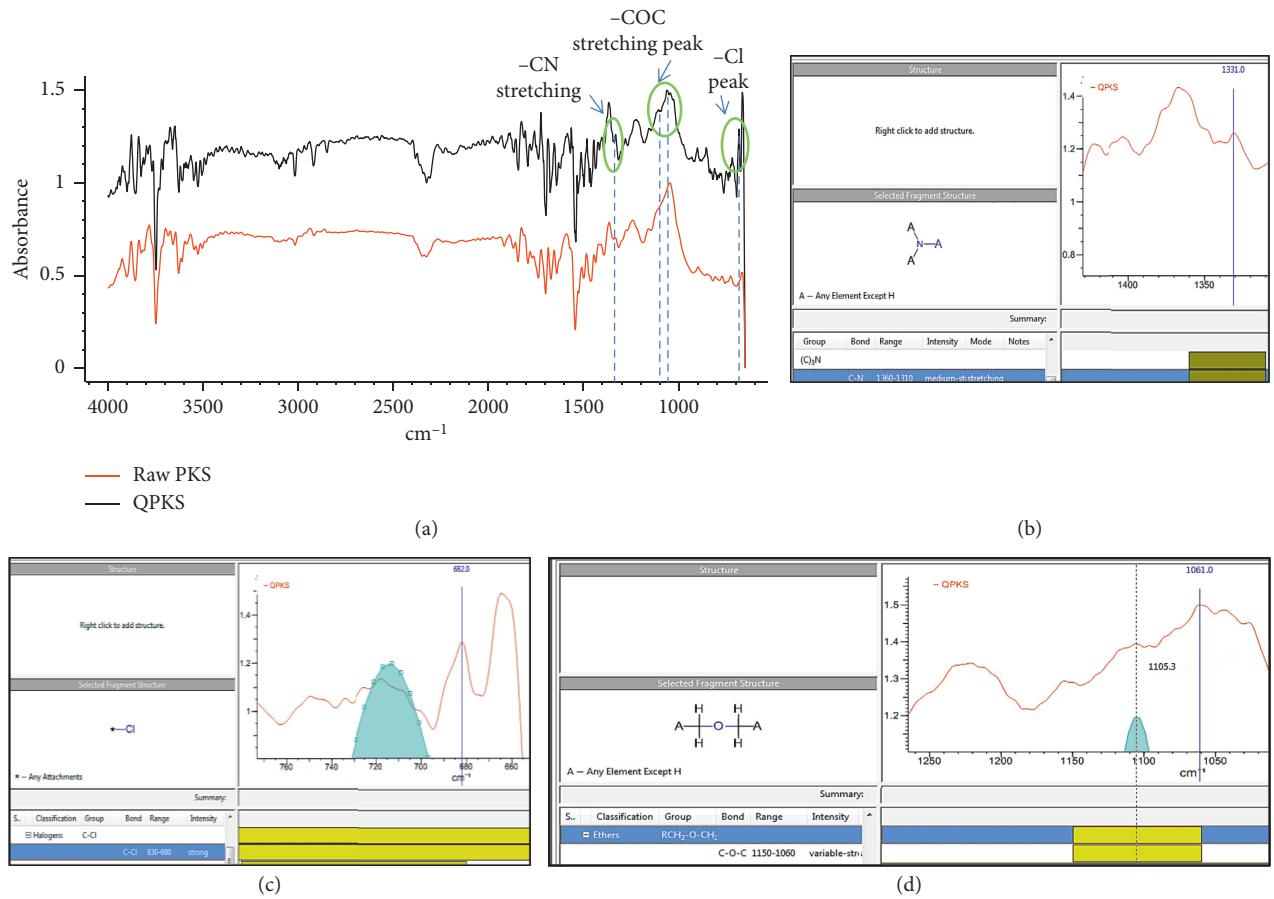

Figure 3: FTIR spectra of (a) raw PKS and QPKS, (b) peak of–CN, (c) peak of Cl, and (d) peak of –COC.

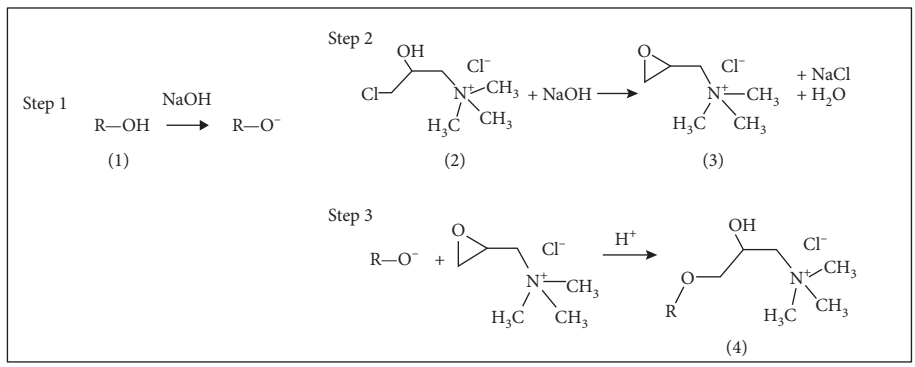

Figure 4: Lignocellulose quaternization reaction scheme: (1) cellulose, (2) *N*-(3-chloro-2-hydroxypropyl), (3) trimethylammonium chloride epoxide, and (4) quaternized cellulose [30].

the breakthrough and exhaust time. Breakthrough occurred when C_t/C_0 was equal to 0.75. Similar trend was observed in fluoride adsorption on manganese oxide coated alumina [36] and on hydrous ferric oxide (HFO) [34]. The area above the breakthrough curve also represented the adsorption capacity of adsorbent [37]. Exhaustion occurred when all active sites on adsorbents were occupied or saturated by adsorbate ions which in this study were the fluoride ions. At this point, final concentration was the same as initial concentration.

At a bed height of 2 cm, the breakthrough time and exhausted time of QPKS were 8.75 minutes and 17.5 minutes. This is due to the porosity effect of each adsorbent in which QPKS has larger pore size as compared to PKSAC which resulted in lower amount of active site on PKSAC to adsorb the fluoride ion. Efficiency and capacity of column adsorption was largely dependent on the amount of adsorbent in the column and porosity. Table 5 shows the breakthrough and exhaustion time for all bed heights.

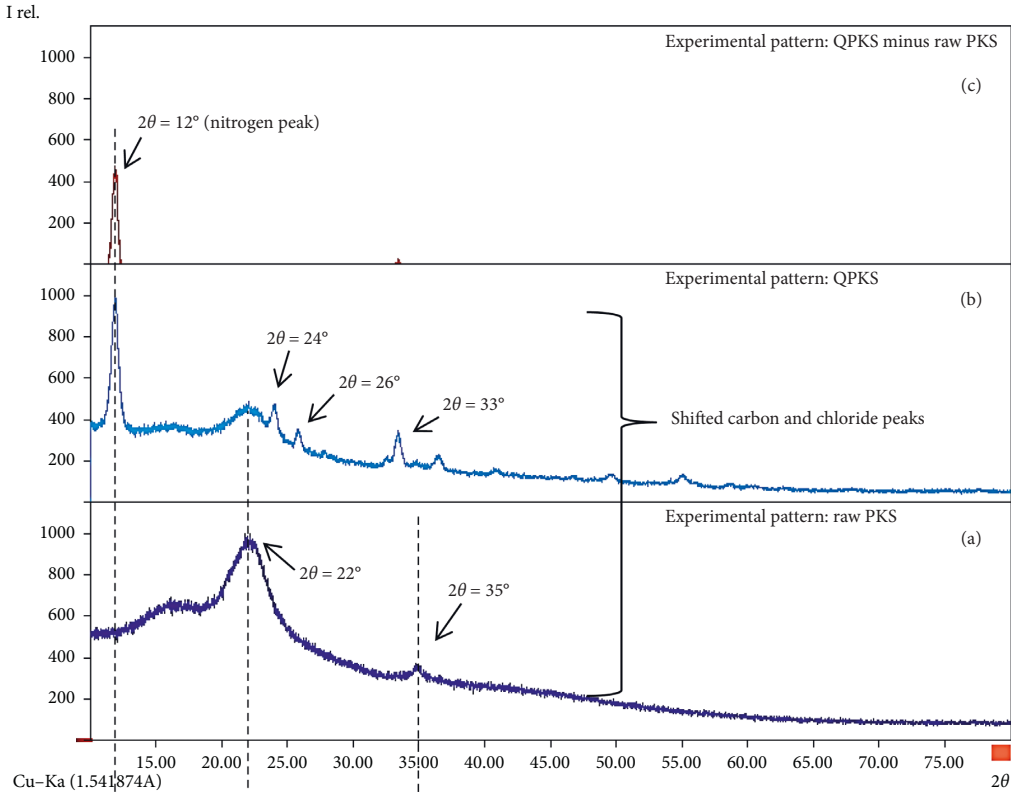

Figure 5: XRD peaks of (a) raw PKS, (b) QPKS, and (c) peak difference between raw PKS and QPKS.

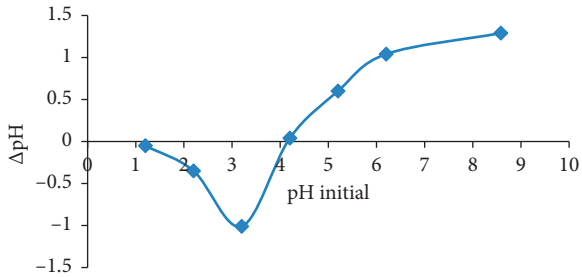

Figure 6: Point of zero charge (pH_{pzc}) of QPKS.

3.4. Kinetic Models

3.4.1. Yoon–Nelson Model. Figure 9 shows the Yoon–Nelson plot on fluoride adsorption at different bed heights and initial concentrations. Values for K_{YN} were determined from the slope, and τ was calculated from the intercept. All the values obtained are compiled in Table 6. K_{YN} values were found to be decreased with the increase of the bed height, and τ values, which are the time required for breakthrough, showed an increasing trend with increasing bed height. It indicated the adsorbate breakthrough was taking longer duration with increasing bed height. These findings were in agreement with the observations reported by Chowdhury et al. [38] and Yadav et al. [39]. Meanwhile, values of K_{YN} were observed to be increased, and τ values decreased with increasing initial fluoride concentration. Chowdhury et al. [38], Nwabanne and Igbokwe [40], and Mohan et al. [25] also reported a similar trend in their work.

3.4.2. Thomas Model. The Thomas model is one of the most general and widely used models to describe the performance theory of the adsorption process in fixed-bed columns. The Thomas model assumed the adsorption process follows Langmuir kinetic. Using equation (1), K_{Th} and q_e were calculated from slope and intercepts of linear plots of $\ln[(C_0/C_t) - 1]$ versus t which are showed in Figure 10 for different bed heights and initial concentrations. Table 7 shows the results of effect of different bed heights and initial fluoride concentrations. K_{Th} values decreased with increased parameter values but q_e values showed increasing trend with increased parameter values. Higher mass transfer driving force was produced by increasing concentration of fluoride ions, therefore increases the concentration gradient and the adsorption capacity [35].

3.4.3. Adams–Bohart and Bed Depth Service Time (BDST) Model. The Adams–Bohart model constants, K_{AB} and N_0, were determined from the plot in Figure 11(a) at different bed heights and at different initial concentrations (Figure 11(b)). All the values are presented in Table 8. The values of R^2 were between 0.59 and 0.98. Table 8 clearly shows that the values of K_{AB} increased with increasing bed height; meanwhile, N_0 decreased as the bed height increased. In contrast, initial fluoride concentration gave the different values for K_{AB} and N_0. As the initial concentration increased,

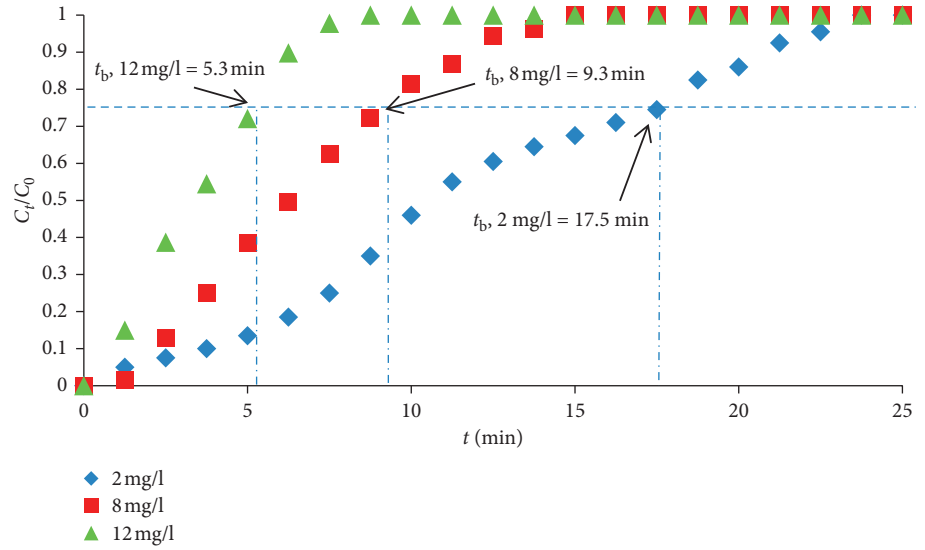

Figure 7: Effect of inlet fluoride concentration on breakthrough profile of QPKS (pH = 3, treated volume = 100 ml, flow rate = 4 ml/min, and bed height = 6 cm).

Table 4: Breakthrough time and exhausted time at different inlet fluoride concentrations.

Initial fluoride concentration (mg/L)	Breakthrough time (min)	Exhausted time (min)
2	17.5	23.75
8	9.3	15
12	5.3	8.75

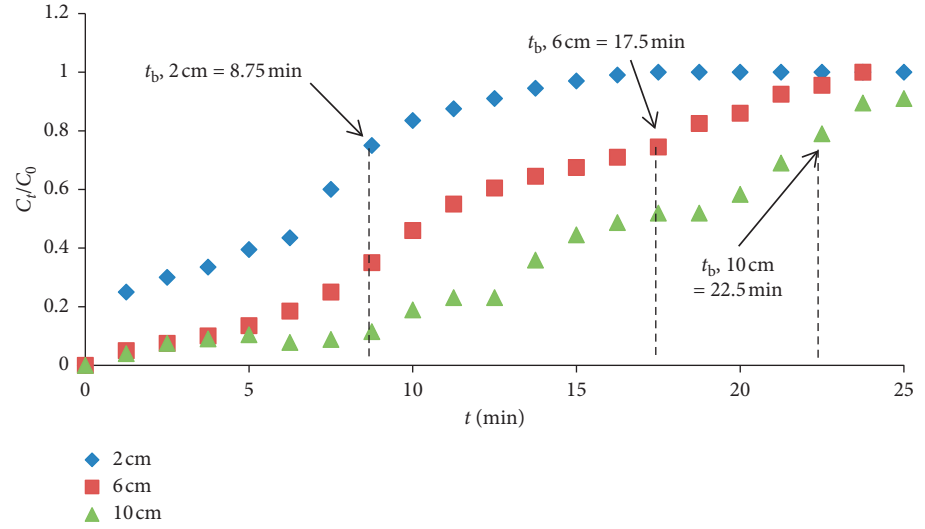

Figure 8: Effect of bed height on breakthrough profile of QPKS (pH = 3, treated volume = 100 ml, flow rate = 4 ml/min, and initial fluoride concentration = 2 mg/l).

Table 5: Breakthrough time and exhausted time at different bed heights.

Bed height (cm)	Breakthrough time (min)	Exhausted time (min)
2	8.75	17.5
6	17.5	23.75
10	22.5	>25

K_{AB} showed the decreasing values but an increasing trend for N_0. The trend is in agreement with the findings reported by the study carried out by Ataei-Germi and Nematollahzadeh [41] who removed methylene blue using nanoparticles and Yadav et al. [39] on fixed-bed fluoride removal by using a commercial Bio-F adsorbent.

According to equation (4), t vs. Z was plotted and is shown in Figure 12 for each adsorbent, where t values were

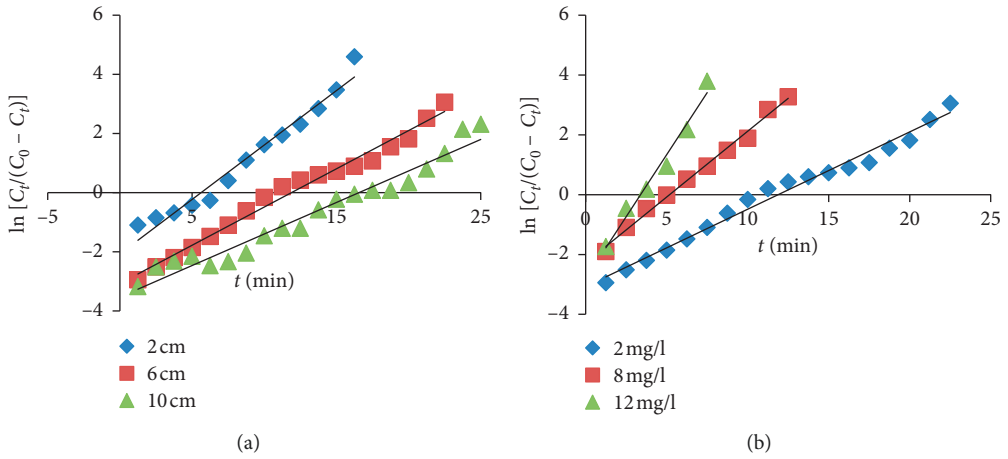

Figure 9: Yoon–Nelson model at different (a) bed heights and (b) initial concentrations by QPKS.

Table 6: Yoon–Nelson constant values at different bed heights and initial concentrations.

Parameter		K_{YN} (min^{-1})	τ (min)	R^2
Bed height (cm)	2	0.3681	5.61994	0.97
	6	0.2586	11.8778	0.98
	10	0.2132	16.55816	0.96
Initial fluoride concentration (mg/L)	2	0.2596	11.8321	0.98
	8	0.4403	5.1787	0.99
	12	0.8302	3.3901	0.98

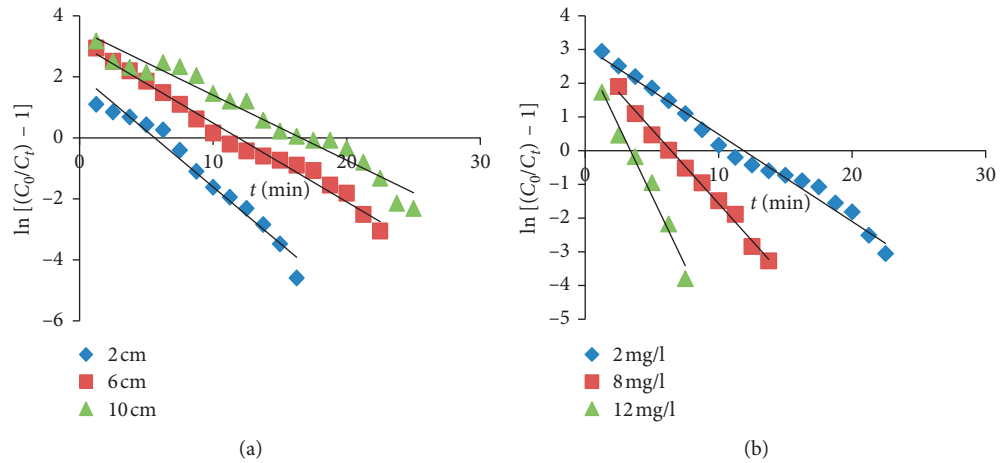

Figure 10: Plot of Thomas model at different (a) bed heights and (b) initial concentrations.

Table 7: Constant values of Thomas model at different bed heights and initial concentrations by QPKS.

Parameter		QPKS		
		K_{Th} (ml/min·mg)	q_e (mg/g)	R^2
Bed height (cm)	2	0.1841	5.6199	0.97
	6	0.1428	10.7549	0.98
	10	0.1066	16.5582	0.96
Initial fluoride concentration (mg/L)	2	0.1293	11.8778	0.98
	8	0.0550	27.9046	0.99
	12	0.0692	22.1989	0.98

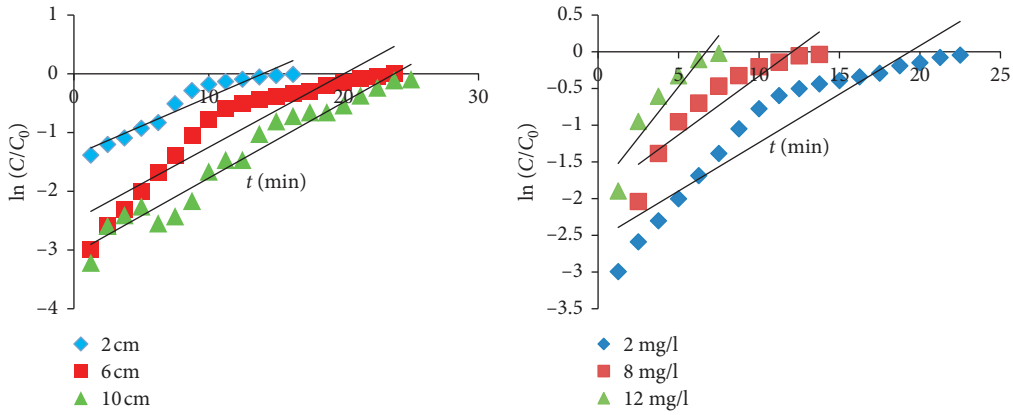

Figure 11: Adams–Bohart model at different (a) bed heights (pH = 3, treated volume = 100 ml, flow rate = 4 ml/min, and initial fluoride concentration = 2 mg/L) and (b) initial fluoride concentrations (pH = 3, treated volume = 100 ml, flow rate = 4 ml/min, and bed height = 6 cm).

Table 8: Adams–Bohart constants at different conditions for the fluoride adsorption by QPKS using linear regression analysis.

Parameter		K_{AB} (L/mg·min)	N_0 (mg/L)	R^2
Bed height (cm)	2	0.049	17.824	0.92
	6	0.062	8.493	0.87
	10	0.065	6.049	0.96
Initial fluoride concentration (mg/L)	2	0.066	8.219	0.88
	8	0.020	20.489	0.85
	12	0.023	17.099	0.87

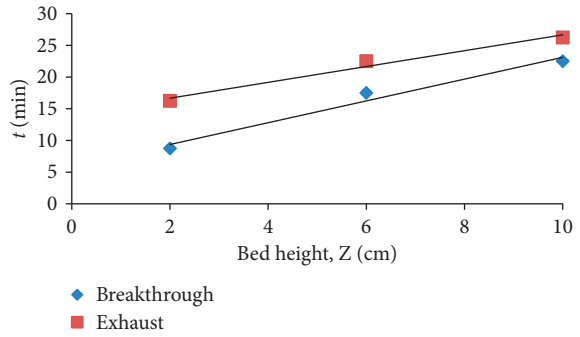

Figure 12: Plot of BDST model of QPKS.

considered for breakthrough times and the exhaust times. The slope of the BDST line represents the time required for the adsorption zone to travel a unit length through the adsorbent under the selected experimental conditions at a given concentration. This can be used to predict the performance of the bed if there is a change in the initial solute concentration. The values of the constants are presented in Table 9, and z_o which is the minimum column height to produce 1.5 mg/L fluoride was found to be 3.45 cm for QPKS.

Different adsorbents produced different adsorption capacities on removing fluoride due to their different properties. Table 10 shows the values of adsorption capacity by using different adsorbent from previous research findings.

Table 9: BDST constant values for QPKS.

Bed height (cm)	Breakthrough time (min)	Exhaust time (min)	N_0 (mg/L)	K	Z_o (cm)
2	8.75	16.25			
6	17.5	22.5	13.7504	−0.0925	3.45
10	22.5	26.25			

Table 10: Comparison of adsorption capacity by different adsorbents on fluoride removal.

Author	Types of adsorbent	Bed height (cm)	Initial concentration (mg/l)	q (mg/g)
Chen et al. [33]	Kanuma mud	10	20	1.56
Nur et al. [34]	Hydrous ferric oxide	12	30	7.06
Paudyal et al. [35]	Zr(IV) loaded dried orange juice residue	4.8	29.3	7.2
Yadav et al. [39]	Bio-F sorbent	10	30	9.87
Talat et al. [42]	Coconut husk activated carbon	5	10	1.3
This study	Quaternized palm kernel shell	6	6	0.99

4. Conclusions

From this study, QPKS prepared was found to be suitable for F^- removal from aqueous solution using continuous adsorption column. Breakthrough time increases with increasing bed height due to increasing amount of the active site on adsorbents to adsorb the fluoride ion. Decreasing trend of breakthrough values was obtained with increasing initial fluoride concentration due to greater driving force for the transfer process to overcome the mass transfer resistance in the column. Kinetic models plotted for fixed-bed column

were Yoon–Nelson, Thomas, Adams–Bohart, and BDST models. Experimental data fit well with Yoon–Nelson with R^2 values between 0.96 and 0.99, a range from 0.96 to 0.99 for the Thomas model, and 0.85 to 0.96 for the Adams–Bohart model. Thus, according to the performance, adsorption capacity, and sustainability on waste management, column adsorption using waste material as adsorbent is best to be used on removing fluoride in both drinking water and wastewater treatment.

Data Availability

The data used to support the findings of this study are available from the corresponding author upon request.

Conflicts of Interest

The authors declare that they have no conflicts of interest.

Acknowledgments

The authors express their sincere gratitude to Chemical and Environmental Engineering Department of University Putra Malaysia and Faculty of Engineering, Technology and Built Environment, UCSI University, for the support given to this research project.

References

[1] F. Shen, X. Chen, P. Gao, and G. Chen, "Electrochemical removal of fluoride ions from industrial wastewater," *Chemical Engineering Science*, vol. 58, no. 3–6, pp. 987–993, 2003.

[2] L. Lv, J. He, M. Wei, D. Evans, and Z. Zhou, "Treatment of high fluoride concentration water by MgAl-CO_3 layered double hydroxides: kinetic and equilibrium studies," *Water Research*, vol. 41, no. 7, pp. 1534–1542, 2007.

[3] Z. Ruan, Y. Tian, J. Ruan et al., "Synthesis of hydroxyapatite/multi-walled carbon nanotubes for the removal of fluoride ions from solution," *Applied Surface Science*, vol. 412, pp. 578–590, 2017.

[4] WHO, *Guidelines for Drinking Water Quality*, World Health Organization, Geneva, Switzerland, 4th edition, 2011.

[5] S. Roy and G. Dass, "Fluoride contamination in drinking water—a review," *Resources and Environment*, vol. 3, no. 3, pp. 53–58, 2013.

[6] M. S. Onyango and H. Matsuda, "Chapter 1 fluoride removal from water using adsorption technique," in *Advances in Fluorine Science*, vol. 2, pp. 1–48, Elsevier, Amsterdam, Netherlands, 2006.

[7] K. Santhy and P. Selvapathy, "Removal of reactive dyes from wastewater by adsorption on coir pith activated carbon," *Bioresource Technology*, vol. 97, no. 11, pp. 1329–1336, 2006.

[8] T. C. Chandra, M. M. Mirna, Y. Sudaryanto, and S. Ismadji, "Adsorption of basic dye onto activated carbon prepared from durian shell: studies of adsorption equilibrium and kinetics," *Chemical Engineering Journal*, vol. 127, no. 1–3, pp. 121–129, 2007.

[9] M. A. Tikki, "Fluoride removal from water – a review," *International Journal of Scientific & Engineering Research*, vol. 5, no. 1, pp. 515–519, 2014.

[10] C. J. Geankoplis, *Transport Processes and Separation Process Principles: Includes Unit Operations*, Prentice-Hall, NJ, USA, 2003.

[11] R. M. C. Viegas, M. Campinas, H. Costa, and M. J. Rosa, "How do the HSDM and Boyd's model compare for estimating intraparticle diffusion coefficients in adsorption processes," *Adsorption*, vol. 20, no. 5-6, pp. 737–746, 2014.

[12] P. Miretzky and A. F. Cirelli, "Fluoride removal from water by chitosan derivatives and composites: a review," *Journal of Fluorine Chemistry*, vol. 132, no. 4, pp. 231–240, 2011.

[13] M. Mohapatra, S. Anand, B. K. Mishra, D. E. Giles, and P. Singh, "Review of fluoride removal from drinking water," *Journal of Environmental Management*, vol. 91, no. 1, pp. 67–77, 2009.

[14] N. Afifah, A. Rahman, M. Ismid, M. Said, and S. Azman, "Carbonized green mussel shell as heavy metal removal," *Malaysian Journal of Civil Engineering*, vol. 29, no. 1, pp. 56–68, 2017.

[15] M. A. Renu, K. Singh, S. Upadhyaya, and R. K. Dohare, "Removal of heavy metals from wastewater using modified agricultural adsorbents," *Materials Today: Proceedings*, vol. 4, no. 9, pp. 10534–10538, 2017.

[16] Z. Li, L. Shao, Z. Ruan, W. Hu, L. Lu, and Y. Chen, "Converting untreated waste office paper and chitosan into aerogel adsorbent for the removal of heavy metal ions," *Carbohydrate Polymers*, vol. 193, pp. 221–227, 2018.

[17] K. Singh, D. H. Lataye, and K. L. Wasewar, "Removal of fluoride from aqueous solution by using low-cost sugarcane bagasse: kinetic study and equilibrium isotherm analyses," *Journal of Hazardous, Toxic, and Radioactive Waste*, vol. 20, no. 3, article 04015024, 2016.

[18] A. B. Ayu Haslija Bt, Y. S. Koay, Y. C. Ching et al., "Removal of fluoride using quaternized palm kernel shell as adsorbents : equilibrium isotherms and kinetic studies," *BioResources*, vol. 11, no. 2, pp. 4485–4511, 2016.

[19] S. Mukherjee, S. Barman, and G. Halder, "Fluoride uptake by zeolite NaA synthesized from rice husk: isotherm, kinetics, thermodynamics and cost estimation," *Groundwater for Sustainable Development*, vol. 7, pp. 39–47, 2018.

[20] H. Hu, L. Yang, Z. Lin, Y. Zhao, X. Jiang, and L. Hou, "A low-cost and environment friendly chitosan/aluminum hydroxide bead adsorbent for fluoride removal from aqueous solutions," *Iranian Polymer Journal*, vol. 27, no. 4, pp. 253–261, 2018.

[21] MPOB, Production of palm kernel shell until November 2017, 2017, http://bepi.mpob.gov.my/index.php/en/statistics/production/177-production-2017/793-production-of-palm-kernel-2017.html.

[22] Y. S. Koay, I. S. Ahamad, M. M. Nourouzi, L. C. Abdullah, and T. S. Y. Choong, "Development of novel low-cost quaternized adsorbent from palm oil agriculture waste for reactive dye removal," *BioResources*, vol. 9, no. 1, 2013.

[23] L. Tofan, C. Paduraru, C. Teodosiu, and O. Toma, "Fixed bed column study on the removal of chromium (III) ions from aqueous solutions by using hemp fibers with improved sorption performance," *Cellulose Chemistry & Technology*, vol. 49, no. 2, pp. 219–229, 2015.

[24] J. J. García-Sánchez, M. Solache-Ríos, V. Martínez-Miranda, and C. Solís Morelos, "Removal of fluoride ions from drinking water and fluoride solutions by aluminum modified iron oxides in a column system," *Journal of Colloid and Interface Science*, vol. 407, pp. 410–415, 2013.

[25] S. Mohan, D. K. Singh, V. Kumar, and S. H. Hasan, "Effective removal of Fluoride ions by rGO/ZrO_2 nanocomposite from aqueous solution: fixed bed column adsorption modelling and

its adsorption mechanism," *Journal of Fluorine Chemistry*, vol. 194, pp. 40–50, 2017.

[26] R. A. Hutchins, "New method simplifies design of activated carbon systems," *Chemical Engineering*, vol. 80, no. 19, pp. 133–138, 1973.

[27] Y. H. Yoon and J. H. Nelson, "Application of gas adsorption kinetics I. A theoretical model for respirator cartridge service life," *American Industrial Hygiene Association Journal*, vol. 45, no. 8, pp. 509–516, 1984.

[28] C. Y. Yin, M. K. Aroua, and W. M. A. W. Daud, "Fixed-bed adsorption of metal ions from aqueous solution on polyethyleneimine-impregnated palm shell activated carbon," *Chemical Engineering Journal*, vol. 148, no. 1, pp. 8–14, 2009.

[29] N. Hasraf, M. Nayan, W. Aizan, W. Abdul, and R. A. Majid, "The effect of mercerization process on the structural and morphological properties of pineapple leaf fiber (PALF) pulp," *Malaysian Journal of Fundamental and Applied Sciences*, vol. 10, no. 1, pp. 12–16, 2014.

[30] A. C. de Lima, R. F. Nascimento, F. F. de Sousa, J. M. Filho, and A. C. Oliveira, "Modified coconut shell fibers: a green and economical sorbent for the removal of anions from aqueous solutions," *Chemical Engineering Journal*, vol. 185-186, pp. 274–284, 2012.

[31] L. B. Railsback, "An explanation of point of zero charge," 2006, http://www.gly.uga.edu/railsback/FundamentalsIndex.html.

[32] A. M. Cardenas-Peña, J. G. Ibanez, and R. Vasquez-Medrano, "Determination of the point of zero charge for electrocoagulation precipitates from an iron anode," *International Journal of Electrochemical Science*, vol. 7, pp. 6142–6153, 2012.

[33] N. Chen, Z. Zhang, C. Feng, M. Li, R. Chen, and N. Sugiura, "Investigations on the batch and fixed-bed column performance of fluoride adsorption by kanuma mud," *Desalination*, vol. 268, no. 1–3, pp. 76–82, 2011.

[34] T. Nur, P. Loganathan, T. C. Nguyen, S. Vigneswaran, G. Singh, and J. Kandasamy, "Batch and column adsorption and desorption of fluoride using hydrous ferric oxide: solution chemistry and modeling," *Chemical Engineering Journal*, vol. 247, pp. 93–102, 2014.

[35] H. Paudyal, B. Pangeni, K. Inoue, H. Kawakita, K. Ohto, and S. Alam, "Adsorptive removal of fluoride from aqueous medium using a fixed bed column packed with Zr(IV) loaded dried orange juice residue," *Bioresource Technology*, vol. 146, pp. 713–720, 2013.

[36] S.-X. Teng, S.-G. Wang, W.-X. Gong, X.-W. Liu, and B.-Y. Gao, "Removal of fluoride by hydrous manganese oxide-coated alumina: performance and mechanism," *Journal of Hazardous Materials*, vol. 168, no. 2-3, pp. 1004–1011, 2009.

[37] W.-C. Tsai, M. D. G. de Luna, H. L. P. Bermillo-arriesgado, C. M. Futalan, J. I. Colades, and M.-W. Wan, "Competitive fixed-bed adsorption of Pb(II), Cu(II), and Ni(II) from aqueous solution using chitosan-coated bentonite," *International Journal of Polymer Science*, vol. 2016, Article ID 1608939, 11 pages, 2016.

[38] Z. Chowdhury, S. Zain, and R. Khan, "Studies of lead (II) cations from aqueous solutions onto granular activated carbon derived from mangostana garcinia," *BioResources*, vol. 7, no. 3, pp. 2895–2915, 2012.

[39] M. Yadav, P. Tripathi, A. Choudhary, U. Brighu, and S. Mathur, "Adsorption of fluoride from aqueous solution by Bio-F sorbent: a fixed-bed column study," *Desalination and Water Treatment*, vol. 57, no. 14, pp. 6624–6631, 2016.

[40] J. T. Nwabanne and P. K. Igbokwe, "Kinetic modeling of heavy metals adsorption on fixed bed column," *International Journal of Environmental Research*, vol. 6, no. 4, pp. 945–952, 2012.

[41] T. Ataei-Germi and A. Nematollahzadeh, "Bimodal porous silica microspheres decorated with polydopamine nanoparticles for the adsorption of methylene blue in fixed-bed columns," *Journal of Colloid and Interface Science*, vol. 470, pp. 172–182, 2016.

[42] M. Talat, S. Mohan, V. Dixit, D. K. Singh, S. H. Hasan, and O. N. Srivastava, "Effective removal of fluoride from water by coconut husk activated carbon in fixed bed column: experimental and breakthrough curves analysis," *Groundwater for Sustainable Development*, vol. 7, pp. 48–55, 2018.